

Giant Enhancement of Air Lasing by Complete Population Inversion in N_2^+

Hanxiao Li,¹ Erik Lötstedt², Helong Li,³ Yan Zhou,¹ Nana Dong,¹ Lunhua Deng,¹ Peifen Lu,¹ Toshiaki Ando²,
Atsushi Iwasaki,² Yao Fu,³ Siqi Wang,³ Jian Wu,^{1,4,*} Kaoru Yamanouchi^{2,†} and Huailiang Xu^{1,3,5,‡}

¹State Key Laboratory of Precision Spectroscopy, East China Normal University, Shanghai 200062, China

²Department of Chemistry, School of Science, The University of Tokyo, 7-3-1 Hongo, Bunkyo-ku, Tokyo 113-0033, Japan

³State Key Laboratory of Integrated Optoelectronics, College of Electronic Science and Engineering, Jilin University, Changchun 130012, China

⁴Collaborative Innovation Center of Extreme Optics, Shanxi University, Taiyuan, Shanxi 030006, China

⁵CAS Center for Excellence in Ultra-intense Laser Science, Shanghai 201800, China



(Received 9 April 2020; accepted 9 July 2020; published 28 July 2020)

A fine manipulation of population transfer among molecular quantum levels is a key technology for control of molecular processes. When a light field intensity is increased to the TW-PW cm^{-2} level, it becomes possible to transfer a population to specific excited levels through nonlinear light-molecule interaction, but it has been a challenge to control the extent of the population transfer. We deplete the population in the $X^2\Sigma_g^+(v=0)$ state of N_2^+ almost completely by focusing a dual-color (800 nm and 1.6 μm) intense femtosecond laser pulse in a nitrogen gas, and make the intensity of N_2^+ lasing at 391 nm enhanced by 5–6 orders of magnitude. By solving a time-dependent Schrödinger equation describing the population transfer among the three lowest electronic states of N_2^+ , we reveal that the $X^2\Sigma_g^+(v=0)$ population is depleted by the vibrational Raman excitation followed by the electronic excitation $A^2\Pi_u(v=2,3,4) \leftarrow X^2\Sigma_g^+(v=1) \leftarrow X^2\Sigma_g^+(v=0)$, resulting in the excessive population inversion between the $B^2\Sigma_u^+(v=0)$ and $X^2\Sigma_g^+(v=0)$ states. Our results offer a promising route to efficient population transfer among vibrational and electronic levels of molecules by a precisely designed intense laser field.

DOI: 10.1103/PhysRevLett.125.053201

Coherent population transfer among quantum levels of an atom or a molecule lies at the heart of a variety of fundamental research such as lasing [1,2], quantum computing [3], and chemical reactions [4–6]. Therefore, tracing population transfer is of particular importance to understand dynamical phenomena of atoms and molecules induced by optical and collisional excitations. Recent studies on mirrorless air lasing [2,7–9] attracted researchers not only because it can be applied to standoff spectroscopy [10], detection of pollutants [11], and diagnosis of molecular dynamics [12–14], but because it can afford an opportunity to monitor how populations are transferred among quantum levels through their optical couplings. Among the air lasing emission lines, the N_2^+ lasing at 391 nm associated with the $B^2\Sigma_u^+(v=0) - X^2\Sigma_g^+(v=0)$ emission induced by an ultrashort intense laser pulse is noteworthy [8,9,15–21] because it provides a unique opportunity to monitor how population is transferred to and from the ground $X^2\Sigma_g^+(v=0)$ state. Indeed, we recently demonstrated that the intensity of the lasing at 391 nm can be enhanced by 2 orders of magnitude using a time-varying polarization pulse [22] and that rotational, vibrational, and electronic modulations of the lasing intensity appear in the time domain [23], both of which

were ascribed to the variation of the population in the ground $X^2\Sigma_g^+(v=0)$ state. It was also shown that the N_2^+ lasing at 391 nm can be enhanced by using a polarization modulated pulse [24], which optimizes simultaneously the ionization of N_2 and the postionization multiple-state coupling in N_2^+ . The importance of the postionization excitation of N_2^+ was suggested by Becker *et al.* [25] based on a comparison between theoretical ionization rates and experimental fluorescence spectra.

In the present study, we demonstrate that the population in the $X^2\Sigma_g^+(v=0)$ state, i.e., the vibrational and electronic ground state, of N_2^+ can be depleted almost completely by the irradiation of a composite femtosecond laser field composed of a polarization-modulated NIR 800-nm field, synthesized by a polarization gating (PG) technique, and an infrared (IR) 1.6- μm field. Our experimental results show that the intensity of the N_2^+ lasing at 391 nm associated with the $B^2\Sigma_u^+(v=0) \rightarrow X^2\Sigma_g^+(v=0)$ emission can be enhanced by 5–6 orders of magnitude as compared with that realized by the irradiation of a linearly polarized 800-nm laser field.

We also perform numerical calculations and reveal that the giant enhancement is ascribed to excessive depletion of the population in the $X^2\Sigma_g^+(v=0)$ state achieved by the

combined action of the PG and IR fields. We find that the IR field induces the vibrational Raman excitation process $X^2\Sigma_g^+(v=1) \leftarrow X^2\Sigma_g^+(v=0)$ followed by $A^2\Pi_u(v=2,3,4) \leftarrow X^2\Sigma_g^+(v=1)$ population transfer, which is induced by the rear part of the PG field. Indeed, the population of the $X^2\Sigma_g^+(v=0)$ state becomes as small as only 2%, resulting in a giant gain in the 391-nm lasing at the $B^2\Sigma_u^+(v=0) - X^2\Sigma_g^+(v=0)$ emission.

The experiments were conducted using a Ti:sapphire laser system (Coherent Astrella) that delivers 35 fs, 800 nm (NIR), 1 kHz laser pulses. The laser beam was split into two. One was used to pump an optical parametric amplifier (TOPAS, OperA Solo) to produce tunable IR pulses in the wavelength range of 1150–1900 nm with the pulse duration of about 45 ± 10 fs. The other was used to produce a PG-modulated pulse using a multiple-order quarter-wave plate (MQW) and a zero-order quarter wave plate (ZQW) [22]. The order of the MQW was seven and its optical axis was fixed at 45° with respect to the polarization direction of the input NIR laser pulses. A motorized delay stage was used to finely tune the temporal delay between the NIR and the IR laser pulses. The NIR and IR laser pulses were then collimated and focused into a gas chamber filled with a high-purity nitrogen gas by an $f = 10$ cm quartz lens. The generated forwardly propagating lasing emission at 391 nm was collected by a fiber head connected to a grating spectrometer (HR2000+, Ocean Optics). The supercontinuum background generated via the filamentation as well as the NIR and IR pump pulses propagating through the output window of the gas cell were blocked by a dichroic mirror. The polarization direction of the PG field at the maximum amplitude was set to be parallel to the polarization direction of the IR pulses.

We employ the composite PG-modulated NIR and IR (PG + IR) field to produce the 391 nm lasing in pure nitrogen gas. As an example, we show in Fig. 1 the forward spectra generated, respectively, with the linearly polarized (LP) NIR laser field, the PG-modulated NIR laser field, and the PG + IR laser field in the linear (a) and logarithm (b) scales, where the spectra generated with the PG and PG + IR fields are attenuated, respectively, by 11 and 21 991 times using different neutral density filters. In this measurement, the gas pressure is set at 80 mbar, and the input NIR and IR laser pulse energies are fixed at 0.44 and 0.17 mJ/pulse, respectively. As has already been reported [22,23,26], the LP and PG-modulated laser fields can produce the self-lasing at 391 nm, and the PG-modulated field [22] and the additional IR field [26] can, respectively, enhance the lasing by about 1–2 orders of magnitude. Surprisingly, as can be clearly seen in Fig. 1, the lasing intensity at 391.4 nm produced by the PG + IR field is enhanced by about 5 orders of magnitude as compared with that produced by the LP field.

In order to examine the mechanism of the enhancement of the lasing intensity at 391.4 nm, we record the N_2^+ lasing

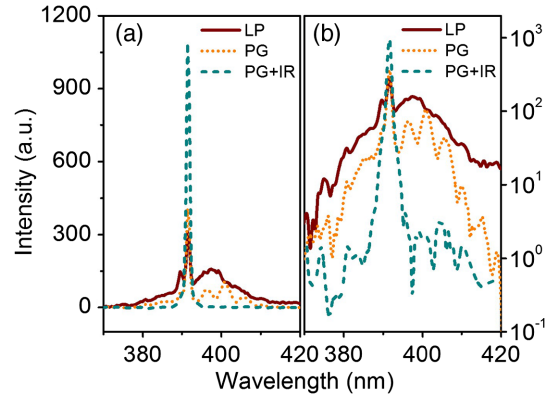


FIG. 1. Strong-field-induced N_2^+ air lasing emissions. The spectra of the forwardly propagating lasing emission peaked at 391.4 nm obtained by the LP (dark red solid line), PG (orange dotted line), and PG + IR (cyan dashed line) cases in the linear (a) and log (b) scales. The intensities of the lasing emissions for the PG and PG + IR cases are attenuated using neutral density filters by 11 and 21 991 times, respectively.

intensity under different experimental conditions. First, we record the lasing intensity as a function of the pulse energy of the incident NIR laser field for the three different cases, that is, the LP, PG, and PG + IR cases. The results are plotted in Fig. 2, in which the LP, PG, and PG + IR cases are represented by blue circles, green triangles, and red squares, respectively. In all three cases, the lasing intensities increase first and then reach saturation as the NIR laser field intensity increases. The first increases in the laser intensity indicate that not only the ionization of N_2 but also the postionization coupling between the $X^2\Sigma_g^+$ and $A^2\Pi_u$ states of N_2^+ are promoted within the same laser pulse [22].

In addition, when the NIR laser field intensity increases, the lasing intensity reaches the saturation much earlier in the PG + IR case than in the LP and PG cases. During the

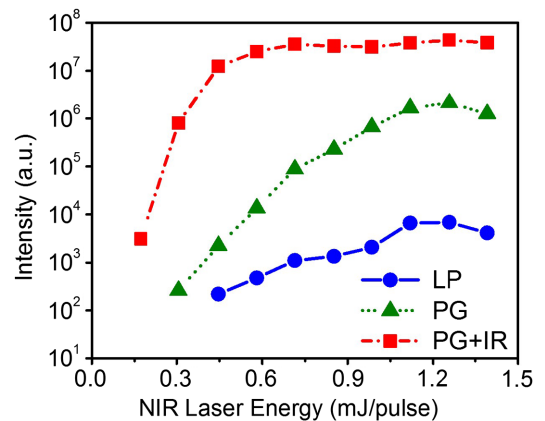


FIG. 2. Lasing intensity versus NIR laser energy. The recorded intensities of lasing at 391 nm generated by the LP (blue circles), PG (green triangles), and PG + IR (red squares) laser fields as a function of the energy of the NIR laser pulse. The pressure of the sample N_2 gas is set to be 70 mbar.

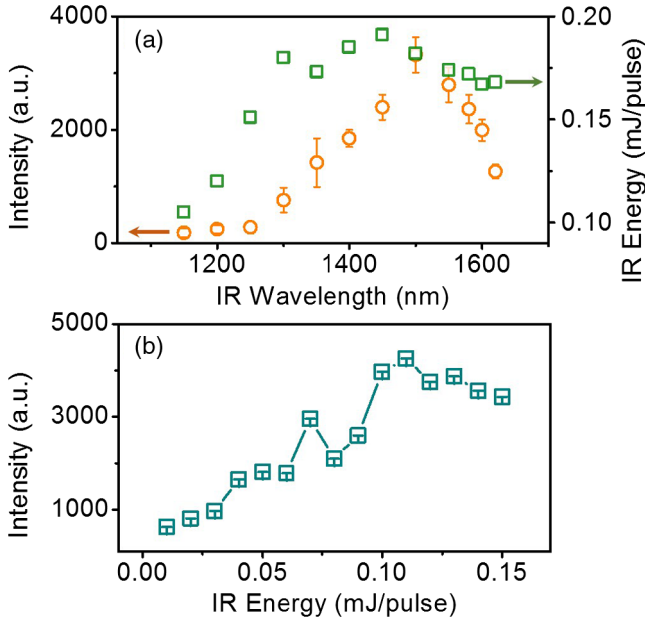


FIG. 3. Lasing intensity versus IR laser wavelength and energy. (a) The recorded intensities of lasing at 391 nm generated by the PG + IR field and the incident IR laser energies as a function of the central wavelength of the IR laser. (b) The recorded intensities of lasing at 391 nm generated by the PG + IR field as a function of the energy of the incident IR laser pulse. For both (a) and (b), the intensity of the NIR PG pulse is kept at 0.44 mJ/pulse and the pressure of the sample N_2 gas is kept at 70 mbar.

fast rise period, the enhancement by 4–5 orders of magnitude is achieved for the PG + IR case as compared with the LP case. It can also be seen in Fig. 2, the threshold energy of the NIR PG laser pulse for the N_2^+ lasing becomes lowered by 0.14 mJ/pulse when the IR laser pulse is introduced, suggesting that the IR laser field depletes further the population in the ground $X^2\Sigma_g^+(v=0)$ state.

Next, for the PG + IR case, we record the intensity of the N_2^+ lasing at 391 nm by changing the wavelength and pulse energy of the incident IR laser pulse while keeping the pressure of the sample N_2 gas at 70 mbar and the energy of the NIR PG laser pulse at 0.44 mJ/pulse. As shown in Fig. 3(a), the enhancement of the lasing intensity can be achieved by the IR laser pulse in the wide IR wavelength range between 1300 and 1600 nm and the most efficient wavelength for the enhancement is around 1500 nm. The enhancement of the lasing intensity at around 1500 nm may be ascribed to slight shortening of the laser pulse duration within the range of 35–55 fs, which enhances nonlinearly the Raman scattering process, transferring the population in the $v=0$ level to the $v=1$ level of the $X^2\Sigma_g^+$ state of N_2^+ . Because of the sudden turn-on behavior of the IR laser field (see Supplemental Material [27]), the effective spectral bandwidth at 1% of the maximum of the amplitude of the IR laser field ($\sim 3095 \text{ cm}^{-1}$) covers the energy separation between the $v=1$ and $v=0$ levels in the $X^2\Sigma_g^+$ state of

N_2^+ , 2175 cm^{-1} , corresponding to the reciprocal of the vibrational period of 15.34 fs, so that the stimulated Raman scattering proceeds.

On the other hand, when we increase the intensity of the IR laser pulse while keeping the wavelength at 1500 nm, the intensity of the NIR PG pulse at 0.44 mJ, and the pressure of the sample N_2 gas at 70 mbar, the N_2^+ lasing intensity increases so that the slope of the increase becomes larger as the IR energy increases until the intensity of the IR laser pulse reaches $\sim 100 \mu\text{J}/\text{pulse}$ as shown in Fig. 3(b) and exhibits a saturation behavior above $\sim 100 \mu\text{J}/\text{pulse}$, indicating that more than one photon of the IR laser light is involved in the enhancement of the lasing intensity at 391 nm.

In order to reveal the mechanism behind the significant enhancement of the lasing at 391 nm by the PG + IR field, we perform numerical simulations of N_2^+ interacting with the PG + IR field based on the postionization three-state coupling model proposed in Ref. [8], in which the $X^2\Sigma_g^+$, $A^2\Pi_u$, and $B^2\Sigma_u^+$ states in N_2^+ are optically coupled by the dipole transitions. We solved the time-dependent Schrödinger equation for the vibronic excitation,

$$i\hbar \frac{\partial}{\partial t} \begin{pmatrix} \psi_X(r, t) \\ \psi_A(r, t) \\ \psi_B(r, t) \end{pmatrix} = [H_0(r) - \mathbf{E}(t) \cdot \mathbf{D}_{AX}(r) - \mathbf{E}(t) \cdot \mathbf{D}_{BX}(r)] \times \begin{pmatrix} \psi_X(r, t) \\ \psi_A(r, t) \\ \psi_B(r, t) \end{pmatrix}, \quad (1)$$

where r is the internuclear distance of N_2^+ , $\psi_\alpha(r, t)$ is the vibrational wave function of the state α ($=X, A, \text{ or } B$), $H_0(r)$ is the field-free Hamiltonian matrix containing the potential energy curves for the respective electronic states, $\mathbf{E}(t)$ is the electric field, and $\mathbf{D}_{\beta X}(r)$ ($\beta = A, B$) is a matrix containing the r -dependent dipole transition matrix elements. The potential energy curves were assumed to take Morse type potentials characterized by experimentally determined vibrational parameters ω_e and $\omega_e x_e$ and the equilibrium internuclear distance r_e [28]. The dipole transition matrix elements were taken from Refs. [29,30]. The rotational motion of N_2^+ was frozen so that the N-N axis is set to be parallel to the polarization direction of the laser pulse at the peak of the pulse ($t=0$). The initial time $t=0$ corresponds to the timing of the ionization at the peak of the laser pulse. At $t=0$, N_2^+ was assumed to be in the electronic ground $X^2\Sigma_g^+$ state with the vibrational wave function of the ground state of neutral N_2 , i.e., $\psi_X(r, t=0) = \chi_{v=0}^{N_2}(r)$ and $\psi_A(r, t=0) = \psi_B(r, t=0) = 0$, corresponding to a prompt ionization $N_2^+ \leftarrow N_2$ according to the Franck-Condon principle. We employed a finite-difference scheme to discretize Eq. (1) in the r variable and a combination of the Lanczos method and the Crank-Nicolson method

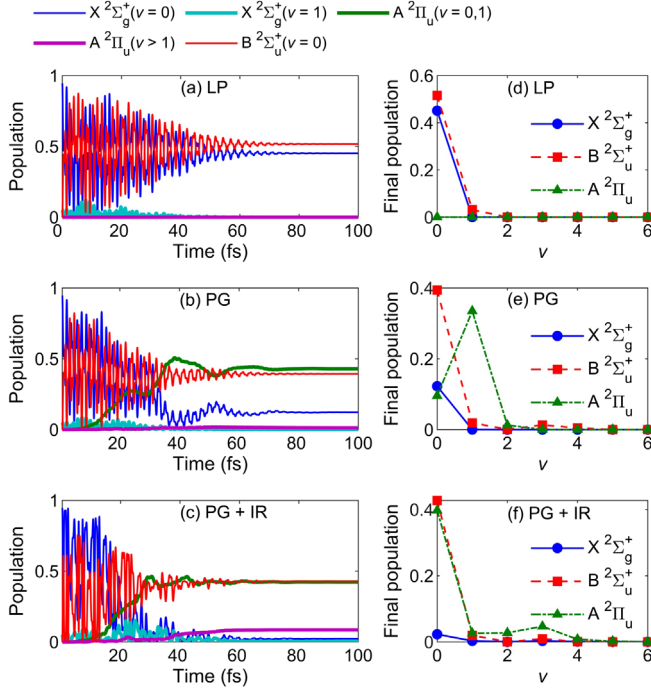


FIG. 4. Population distributions in the vibrational and electronic states of N_2^+ . The time-dependent populations in the $X^2\Sigma_g^+(v=0)$ (blue solid line), $X^2\Sigma_g^+(v=1)$ (light blue solid line), $A^2\Pi_u(v=0, 1)$ (green solid line), $A^2\Pi_u(v > 1)$ (purple solid line), and $B^2\Sigma_u^+(v=0)$ (red solid line) levels are shown for the LP (a), PG (b), and PG + IR (c) cases, and the final populations in the respective vibrational levels at $t = 100$ fs are shown for the LP (d), PG (e), and PG + IR (f) cases. The laser field intensities for the NIR (800 nm) LP and PG pulses are $3.2 \times 10^{14} \text{ W cm}^{-2}$ and the laser field intensity of the IR (1580 nm) pulse is $1.07 \times 10^{14} \text{ W cm}^{-2}$.

for the time stepping. The time-dependent population $p[(\alpha(v), t)]$ in the v th vibrational level in the electronic state α is defined as

$$p[(\alpha(v), t)] = |\langle \psi_\alpha(r, t) | \chi_{av}(r) \rangle|^2, \quad (2)$$

where $\chi_{av}(r)$ is the v th vibrational eigenstate in the electronic state α . Further details on the theoretical model can be found in Ref. [31].

We calculate the time-dependent populations in the respective states after the creation of N_2^+ upon the ionization. One example of the population dynamics is shown in Fig. 4, where the time-dependent [Figs. 4(a)–4(c)] and final [Figs. 4(d)–4(f)] populations in the vibrational states of the $X^2\Sigma_g^+$, $A^2\Pi_u$, and $B^2\Sigma_u^+$ states are shown for the LP (800 nm), PG (800 nm), and PG (800 nm)+IR (1580 nm) cases. The polarization direction of the linearly polarized IR pulse is set to be parallel to the polarization direction of the PG pulse at the timing when the PG pulse takes the maximum intensity. The N-N molecular axis of N_2^+ is assumed to be parallel to the polarization direction of the PG pulse at the

peak of the pulse for the simulations with PG and PG + IR pulses, and parallel to the polarization direction of the LP pulse for simulations with the LP pulse. The laser field intensities of the LP and PG pulses are set to be $3.2 \times 10^{14} \text{ W cm}^{-2}$ and the laser field intensity of the IR pulse is set to be $1.1 \times 10^{14} \text{ W cm}^{-2}$. The pulse widths (FWHM) of all the LP, PG, and IR pulses are set to be 40 fs.

We can see in Fig. 4 that, while population inversion is achieved for all the three cases, the extent of the population inversion is the largest in the PG + IR case. Indeed, the final populations in the $X^2\Sigma_g^+(v=0)$ level are $p_{\text{LP}}[X(v=0)] = 45\%$, $p_{\text{PG}}[X(v=0)] = 12\%$, and $p_{\text{PG+IR}}[X(v=0)] = 2.3\%$ for the LP, PG, and PG + IR cases, respectively, and the final populations in the $B^2\Sigma_u^+(v=0)$ level are $p_{\text{LP}}[B(v=0)] = 52\%$, $p_{\text{PG}}[B(v=0)] = 39\%$, and $p_{\text{PG+IR}}[B(v=0)] = 43\%$ for the LP, PG, and PG + IR cases, respectively. Therefore, the final population differences between the $B^2\Sigma_u^+(v=0)$ and $X^2\Sigma_g^+(v=0)$ levels are $\Delta p_{\text{LP}} = 6.5\%$, $\Delta p_{\text{PG}} = 27\%$, and $\Delta p_{\text{PG+IR}} = 40\%$ for the LP, PG, and PG + IR cases, respectively.

As can be seen in Fig. 4(c), the IR field induces the vibrational excitations in the time interval of $20 \text{ fs} < t < 40 \text{ fs}$ through the Raman pumping processes represented by the scheme of $X^2\Sigma_g^+(v=1) \leftarrow X^2\Sigma_g^+(v=0)$ through the polarization tensor composed of the dipole coupling between the $X^2\Sigma_g^+$ and $B^2\Sigma_u^+$ states. The total population in the $X^2\Sigma_g^+(v > 1)$ states is smaller than 3% when $t < 100$ fs, while the maximum value of the population in the $X^2\Sigma_g^+(v=1)$ state, which is taken at $t = 23$ fs, is 17%. The population in the $X^2\Sigma_g^+(v=1)$ state is then subsequently transferred to the vibrationally excited $A^2\Pi_u(v=2, 3, 4)$ states by the $A^2\Pi_u$ - $X^2\Sigma_g^+$ dipole transitions induced by the electric field component of the PG pulse perpendicular to the N-N molecular axis. The numerical simulations show clearly that the giant enhancement of the intensity of the lasing at 391 nm realized by the PG-IR laser field is achieved by the depletion of the population in the $X^2\Sigma_g^+(v=0)$ level through the vibrational Raman pumping within the $X^2\Sigma_g^+$ state promoted by the IR laser field followed by the efficient population transfer to the vibrationally excited levels in the $A^2\Pi_u$ state by the NIR PG field (see Supplemental Material [27]).

Furthermore, the numerical simulations also show that the transfer of the population from the $A^2\Pi_u$ state to the $B^2\Sigma_u^+$ state, which may be induced by the IR laser field via a two-photon transition, is of limited importance because the final population in the $B(v=0)$ level for the PG + IR case, $p_{\text{PG+IR}}[B(v=0)] = 43\%$, is almost the same as that for the PG case, $p_{\text{PG}}[B(v=0)] = 39\%$. In order to make a more quantitative comparison of the theoretical results with the experimental ones, more extensive theoretical simulations have to be performed, in which the molecular alignment angle and the ionization timing are varied by

taking into account the angle-dependent and time-dependent ionization probabilities.

In conclusion, we have shown experimentally that the intensity of the $B^2\Sigma_u^+(v=0) - X^2\Sigma_g^+(v=0)$ lasing line of N_2^+ at 391 nm is enhanced by 5–6 orders of magnitude by the dual-color intense ultrashort laser field composed of a NIR laser pulse whose polarization direction varies temporally and a linearly polarized IR laser pulse. We have identified the mechanism of this giant enhancement of the lasing intensity at 391 nm by the numerical simulations of the population transfers based on the $X^2\Sigma_g^+$, $A^2\Pi_u$, $B^2\Sigma_u^+$ three-state coupling in the dual-color intense laser field. The mechanism is the following: First, N_2^+ is created within the laser field through the sudden turn-on scheme [8] through which a certain amount of the population is transferred to the $B^2\Sigma_u^+(v=0)$ level. Next, the IR laser field depletes the population in the $X^2\Sigma_g^+(v=0)$ level to the vibrationally excited $v=1$ level in the $X^2\Sigma_g^+$ state through the vibrational Raman and sequential vibrational Raman pumping. Finally, the NIR PG field transfers the population in the vibrationally excited $v=1$ level in the $X^2\Sigma_g^+$ state to the vibrationally excited levels in the $A^2\Pi_u$ state. Indeed, the numerical calculations show that the population in the $X^2\Sigma_g^+(v=0)$ level can be as small as 2% while the population in the $B^2\Sigma_u^+(v=0)$ level is 43%, resulting in a huge enhancement of the lasing signal, which we observe experimentally. Our results not only clarify the mechanism of the giant enhancement of the N_2^+ lasing at 391 nm but also demonstrate that fine manipulations of the population in quantum levels of molecules can be achieved by an optimally designed intense laser field through the combination of various types of vibrational and electronic transitions.

This work was supported in part by the National Natural Science Foundation of China (NSFC) (No. 61625501, No. 61427816, No. 11834004, and No. 11761141004), the National Key R&D Program of China (2018YFA0306303), the two MEXT (Ministry of Education, Culture, Sports, Science and Technology) Grant-in-Aid for Specially Promoted Research (No. 19002006 and No. 15H05696), the 111 project of China (Grant No. B12024), and Projects from the Shanghai Science and Technology Commission (19JC1412200).

*jwu@phy.ecnu.edu.cn

†kaoru@chem.s.u-tokyo.ac.jp

‡huailiang@jlu.edu.cn

- [1] O. Svelto and D. Hanna, *Principles of Lasers*, 4th ed. (Plenum Press New York, 1999).
- [2] A. Dogariu, J. B. Michael, M. O. Scully, and R. B. Miles, *Science* **331**, 442 (2011).
- [3] C.-W. Chou, C. Kurz, D. B. Hume, P. N. Plessow, D. R. Leibbrandt, and D. Leibfried, *Nature (London)* **545**, 203 (2017).
- [4] E. D. Potter, J. L. Herek, S. Pedersen, Q. Liu, and A. H. Zewail, *Nature (London)* **355**, 66 (1992).
- [5] J. R. Clarkson, E. Baquero, V. Alvin Shubert, E. M. Myshakin, K. D. Jordan, and T. S. Zwier, *Science* **307**, 1443 (2005).
- [6] A. S. Alnaser *et al.*, *Nat. Commun.* **5**, 3800 (2014).
- [7] Q. Luo, W. Liu, and S. L. Chin, *Appl. Phys. B* **76**, 337 (2003).
- [8] H. Xu, E. Lötstedt, A. Iwasaki, and K. Yamanouchi, *Nat. Commun.* **6**, 8347 (2015).
- [9] J. Yao *et al.*, *Phys. Rev. Lett.* **116**, 143007 (2016).
- [10] P. R. Hemmer, R. B. Miles, P. Polynkin, T. Siebert, A. V. Sokolov, P. Sprangle, and M. O. Scully, *Proc. Natl. Acad. Sci. U.S.A.* **108**, 3130 (2011).
- [11] P. N. Malevich, R. Maurer, D. Kartashov, S. Ališauskas, A. A. Lanin, A. M. Zheltikov, M. Marangoni, G. Cerullo, A. Baltuška, and A. Pugžlys, *Opt. Lett.* **40**, 2469 (2015).
- [12] H. Zhang *et al.*, *Phys. Rev. X* **3**, 041009 (2013).
- [13] H. Xie *et al.*, *Phys. Rev. A* **90**, 042504 (2014).
- [14] M. Lei, C. Wu, A. Zhang, Q. Gong, and H. Jiang, *Opt. Express* **25**, 4535 (2017).
- [15] J. Yao, B. Zeng, H. Xu, G. Li, W. Chu, J. Ni, H. Zhang, S. Chin, Y. Cheng, and Z. Xu, *Phys. Rev. A* **84**, 051802(R) (2011).
- [16] T. Wang, J. Ju, J. Daigle, S. Yuan, R. Li, and S. Chin, *Laser Phys. Lett.* **10**, 125401 (2013).
- [17] Y. Liu, P. Ding, N. Ibrakovic, S. Bengtsson, S. Chen *et al.*, *Phys. Rev. Lett.* **119**, 203205 (2017).
- [18] A. Azarm, P. Corkum, and P. Polynkin, *Phys. Rev. A* **96**, 051401(R) (2017).
- [19] L. Arissian, B. Kamer, A. Rastegari, D. M. Villeneuve, and J. C. Diels, *Phys. Rev. A* **98**, 053438 (2018).
- [20] X. Zhong, Z. Miao, L. Zhang, Q. Liang, M. Lei, H. Jiang, Y. Liu, Q. Gong, and C. Wu, *Phys. Rev. A* **96**, 043422 (2017).
- [21] A. Zhang *et al.*, *Opt. Express* **27**, 12638 (2019).
- [22] H. Li, M. Hou, H. Zang, Y. Fu, E. Lötstedt, T. Ando, A. Iwasaki, K. Yamanouchi, and H. Xu, *Phys. Rev. Lett.* **122**, 013202 (2019).
- [23] T. Ando, E. Lötstedt, A. Iwasaki, H. L. Li, Y. Fu, S. Wang, H. L. Xu, and K. Yamanouchi, *Phys. Rev. Lett.* **123**, 203201 (2019).
- [24] Y. Fu, E. Lötstedt, H. Li, S. Wang, D. Yao, T. Ando, A. Iwasaki, F. H. M. Faisal, K. Yamanouchi, and H. Xu, *Phys. Rev. Research* **2**, 012007(R) (2020).
- [25] A. Becker, A. D. Bandrauk, and S. L. Chin, *Chem. Phys. Lett.* **343**, 345 (2001).
- [26] J. Chen *et al.*, *Phys. Rev. A* **100**, 031402(R) (2019).
- [27] See Supplemental Material at <http://link.aps.org/supplemental/10.1103/PhysRevLett.125.053201> for an explanation of the mechanism of the stimulated Raman process induced by the IR pulse.
- [28] K. P. Huber and G. H. Herzberg (data prepared by J. W. Gallagher and R. D. Johnson, III), *Constants of Diatomic Molecules*, in *NIST Chemistry WebBook, NIST Standard Reference Database Number 69*, edited by P. J. Linstrom and W. G. Mallard (National Institute of Standards and Technology, Gaithersburg MD, 2019).
- [29] S. R. Langhoff, C. W. Bauschlicher, Jr., and H. Partridge, *J. Chem. Phys.* **87**, 4716 (1987).
- [30] S. R. Langhoff and C. W. Bauschlicher, Jr., *J. Chem. Phys.* **88**, 329 (1988).
- [31] H. Xu, E. Lötstedt, T. Ando, A. Iwasaki, and K. Yamanouchi, *Phys. Rev. A* **96**, 041401(R) (2017).